2

The BESSY Raytrace Program RAY

F. Schäfers

Abstract. The raytracing program RAY simulates the imaging properties of an optical system. It randomly creates a set of rays within various types of light sources and traces them according to the laws of geometric optics through optical elements onto image planes. The distribution of the rays at the source, optical elements and image planes can be displayed.

A ray is described not only by its coordinates with respect to a suitable coordinate system, but also by its energy and its polarisation determined by the Stokes vector. Different source types are implemented with special emphasis on a realistic simulation of source intensity, volume and emission characteristics, especially for synchrotron radiation including dipole and undulator sources. Optical elements can be reflection mirrors of nearly any figure (plane, cylindrical, spherical, aspherical...), gratings, zone plates, foils or crystals. The absolute transmission of the optics including the effect of optical (multilayered) coatings is calculated according to the reflection/refraction/transmission process from the optical constants of the materials involved. The influence of misalignment of the source and/or the optical elements, slope errors and thermal deformation of the optics can also be taken into account. A graphical display of spot patterns at any position of the beam, intensity and angular distributions, absolute flux, polarisation, energy resolution is possible.

2.1 Introduction

The development of the raytracing program RAY was started at BESSY in 1984 for basic raytracing calculations of VUV- and soft X-ray optical schemes [1]. Since that time RAY has been in continuous evolution and it has grown into a widely used design tool for synchrotron radiation beamlines as well as for other optical systems. Most of the BESSY I monochromators have been designed using RAY. To meet the requirements of the new undulator-based third generation storage ring BESSY II, many new features have been implemented into the code in the last 10 years such that RAY now has become an indispensable tool for modern beamline design. Its capabilities are similar to the widely used $SHADOW$–XOP program [2,3]. Considerable effort has

been made to ensure that it is a user friendly, easy accessable and easy-to-learn program for everyday use with a minimum effort on data and file handling.

Alternative to these programs based on *intensity* distributions and *geometric optics, wavefront* propagation codes have been developed such as *PHASE* [4], which applies the Stationary Phase Approximation and *SRW* [5] employing Fourier Optics, which on the basis of the complex electric field of the radiation are able to intrinsically take into account interference and coherence effects. These codes are treated separately in this book [6].

This report is intended to be a practical reference and to give an outline of the underlying geometrical, mathematical, physical and optical principles which can be found in textbooks [7–9] or synchrotron radiation handbooks [10]. In particular, Chap. 3.2 of [10] (Ray tracing) is strongly recommended as an introductory guide before calculating a real beamline design. Here the procedure, problems, limitations and the importance of *checking* the raytrace results for the various kinds of errors that can occur are discussed. Various specific *RAY*-features have been described previously: crystal optics in [11] and zoneplate optics employing Fresnel diffraction where the collective effects are treated on a statistical (Monte Carlo) basis [12, 13]. Extended manuals for *RAY* [14] and the reflectivity program *REFLEC* [15] which share the same optics software library are also available. Examples for the use of the program in a variety of synchrotron radiation applications are given in [16]: plane grating monochromator (PGM-) beamlines, [17] IR-beamlines, [18] elliptical undulator beamlines, [19] gradient crystal monochromators, [20] µ-focus X-ray beamline.

Chapter 3 explains the basic statistical treatment to simulate any kind of intensity patterns, while the next chapters describe the simulation of sources (Chap. 4), optical elements (Chap. 5) and of the treatment of absolute reflectivity and polarisation (Chap. 6).

In Chap. 7 crystal diffraction optics employing dynamical theory is described. Looking ahead, in 'Outlook', the time evolution of the rays to describe wave, coherence and interference phenomena is discussed (Chap. 8). This extension of the program and the implementation of the zoneplate optics [12, 13] have been made possible by support through the COST-P7 action and intensive discussions during the COST meetings.

The complete code is available as a PC-Windows version.

2.2 Beamline Design and Modelling

The raytracing program *RAY* simulates the imaging and focussing properties of an optical system. It randomly creates a set of rays within various types of light sources and traces them through one or more optical elements on image planes. The geometric distribution of the rays at the source, at all optical elements and at the image planes can be visualized.
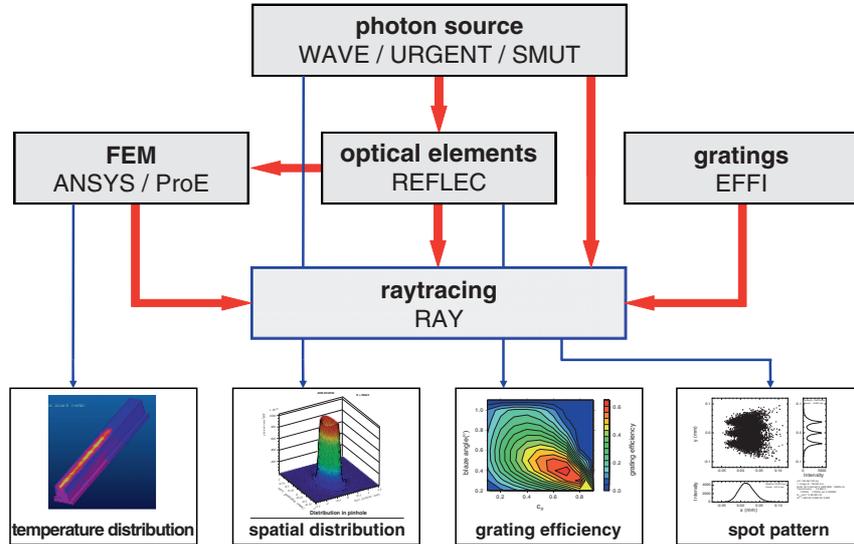
Fig. 2.1. BESSY soft X-ray computational tools and their interplay

Various interesting features like focal properties, power distribution, energy resolution, rocking curves, absolute transmission and polarisation characteristics of an optical setup are simulated. It combines pure geometrical raytracing with calculations of the absolute transmission and is, thus, a central and indispensable part of the BESSY software tools for the design and optimization of new monochromators and beamlines from the infrared spectral region to the hard X-ray range. The interplay of the software tools available at BESSY [21, 22], is demonstrated in Fig. 2.1 as a flowchart.

Special emphasis was put on realistic simulations of beamlines, in particular those employing synchrotron radiation: the path of the photons can be followed from any source, including bending magnets and insertion devices via reflection/diffraction/transmission at optical elements through apertures, entrance and/or exit slits on the sample. The influence of slope errors, surface roughness, thermal bumps, measured or calculated surface profiles as well as a misalignment of the source and optical elements can be studied in a simple way. Thus, it is possible to predict the real performance of the beamline under realistic conditions and to specify the requirements for all the components to be ordered.

In a well defined source volume, rays are created within a given horizontal and vertical divergence. Each ray has the same intrinsic probability. The spatial and angular intensity *distribution* of the source is given by the spatial and angular *density* of the rays (i.e. rays per volume and solid angle). Thus, the outgoing rays simulate the intensity distribution of the corresponding source. The rays are traced according to geometrical optics through one or more optical elements (mirrors, gratings, foils, crystals, slits, zoneplates)

of which the surface can have nearly any figure such as plane, cylindrical, spherical, toroidal, paraboloidal or ellipsoidal and can be arranged in any geometry (horizontal, vertical, oblique). The absolute transmission of the optics including the effect of (multilayer-) coatings is calculated according to the reflection/refraction/transmission/diffraction processes from the optical constants of the involved materials. Special monochromator mounts and (coma-corrected) varied line-spacing (VLS-) gratings and (graded) crystals with automatic calculation of structure factors can also be handled.

A ray is determined not only by its coordinates with respect to a suitable coordinate system (e.g. by its starting point) and by its direction, but also by its energy E, its polarisation, described by the Stokes vector $S = (S_0, S_1, S_2, S_3)$, and its pathlength. Thus, a ray is described by 12 parameters, which are traced through the optical setup and for which the geometrical and optical modifications are calculated according to its interaction with the optical coating (reflection/refraction/transmission). Since all rays have equal probability (the intensity of a ray, S_0, is either 1 or 0), the throughput of a beamline is simply given by the number of rays, for SR-sources multiplied with the absolute photon flux as scaling factor.

For a first overview of the focal properties of an optical system, the horizontal and vertical widths of the beam can be visualized along the beam path for the determination of the focus position. At any position along the beam path image planes can be defined. The footprints of the rays on the optical elements and the focal properties of the optical system are analyzed and are visualized graphically as point diagrams, 2D or 3D intensity distributions etc.

The menu-driven program is user friendly and so a first-performance test of an optical design can be gained rapidly without any file handling. Once the beamline has been defined the parameters are stored and can be modified in a subsequent run. The graphics output is directed to monitors, printers, or PS or EPS-files, and alternatively ASCII-data tables of all results can be created for further data evaluation and display.

A flowchart of the program is shown in Fig. 2.2.

2.3 Statistics: Basic Laws of RAY

2.3.1 All Rays have Equal Probability

To simulate realistic intensity patterns on optical elements and image planes (e.g. for heat load studies) it is necessary to create the source points and the rays in such a way that the same intensity is attributed to each ray.

Generally there are two possibilities:

- A *systematic* distribution of the rays within the source so that the real emission characteristic is simulated. For this a large number of rays is required and needs to be calculated before an optical setup is completely described.
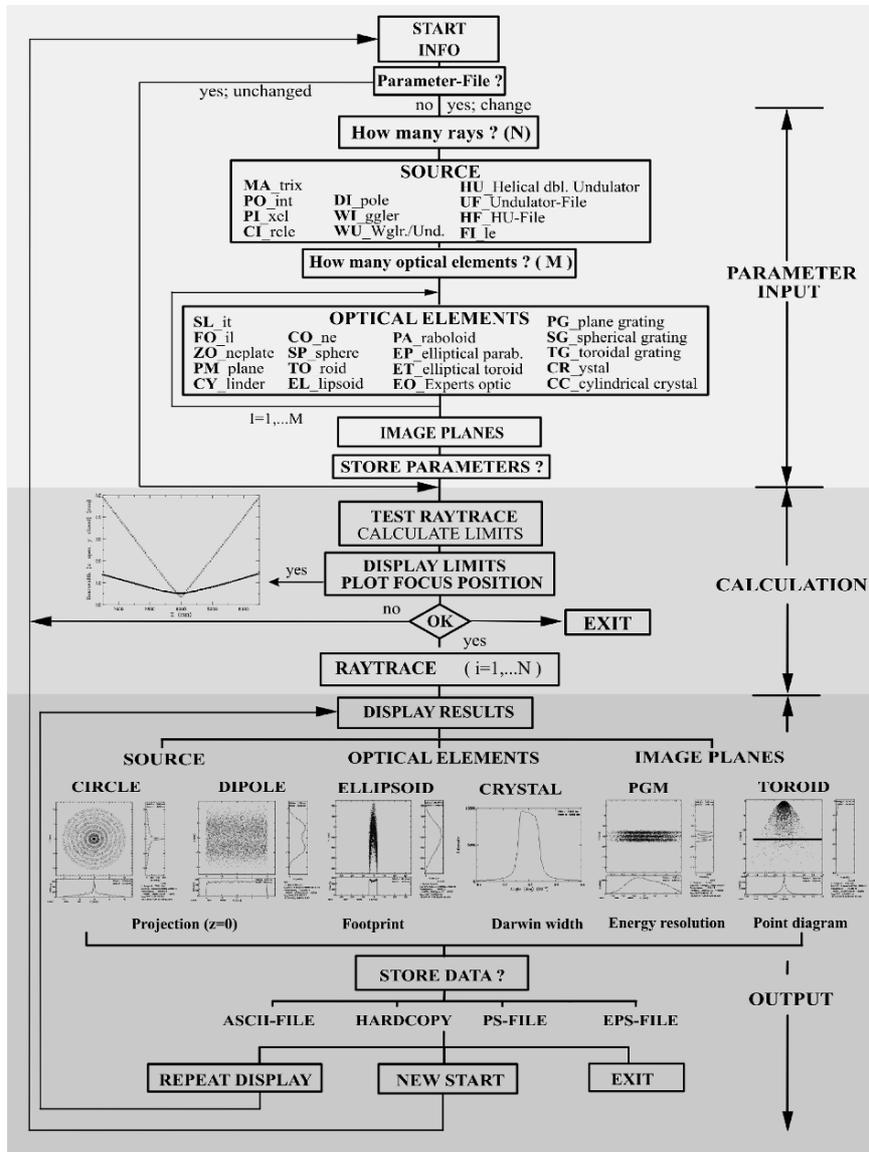
Fig. 2.2. Flow chart of RAY

- The rays are distributed *statistically* within the source so that within the statistical error the real emission characteristic is simulated. The intensity distribution of the source is thus understood as the probability distribution of the necessary parameters, namely position and angle. The main advantages of this Monto–Carlo procedure are its simplicity and the fact that a calculation of relatively few rays already is enough to create a reasonable

simulation of the optics. When the statistics and the accuracy seem to be sufficient, the calculation can always be interrupted without making a systematic error.

This second option is realized in *RAY. T*he procedure is as follows:

1. Create a random number ran_1 between 0 and 1.
2. Scale the corresponding variable, e.g. the x-coordinate of the source point:

$$x = (ran_1 - 0.5)\,\mathrm{d}x, \qquad (2.1)$$

   where $\mathrm{d}x$ is the source-dimension in the x-direction.
3. Calculate the probability, w, of this randomly chosen start value for x (normalized to a maximum value of 1), for example the electron density in a dipole-source (gaussian profile $w(x) = \exp(-x^2/(2\sigma_\mathrm{y}^2))$) or the synchrotron radiation intensity for a fixed wavelength at a definite horizontal and vertical emission angle (Schwinger theory [23]).
4. Create a second random number ran_2. The ray is accepted only if the difference of the probability $w(x)$ and this new random number is larger than zero:

$$w(x) - ran_2 > 0. \qquad (2.2)$$

5. If the difference is less than zero neglect this ray and start again with a new one according to (2.1).

2.3.2 All Rays are Independent, but... (Particles and Waves)

All rays are independent, and so they are considered as individual particles not knowing anything about each other. Thus, *RAY* works exclusively in the particle model. Nevertheless, the statistical method explained above is an elegant way to overcome the particle–wave dualism and to simulate wave phenomena and collective effects such as interference, diffraction, coherence and wave fronts.

This is done by a statistical treatment of an ensemble of individual rays which behave within the statistical errors as a collective unit, as a wavefront.

This random selection of a parameter is used extensively throughout the program not only to simulate the emission characteristics of a light source, but also, for example, to simulate the reflection angle on a mirror to simulate slope errors that are assumed to be gaussian. It is used to simulate reflection losses of rays where $w(x) = R$ with $(0 < R < 1)$ by which the surviving ray is assigned a probability of 1.

Furthermore, it is applied to simulate diffraction effects on slits for which the outgoing beam direction is modulated by a $\sin v/v$ term for the case of rectangular slits or by a bessel function for the case of circular slits.

The same diffraction routine is used for zone plate optics to simulate airy patterns at the focus point in first, third and fifth harmonic [12, 13].

2.4 Treatment of Light Sources

Various light sources are incorporated in *RAY*. Generally the rays are starting in a defined source volume and are emitted with a defined horizontal and vertical divergence. Either hard (flat-top) edges or a gaussian distribution profile can be simulated. In the latter case, rays are created statistically (see 3.1) within a $\pm 3\sigma$-width of the gaussian profile (i.e. more than 99.9% of the intensity).

For synchrotron radiation beamlines, the polarised emission characteristic of bending magnets, wigglers and undulators is incorporated. For other sources, such as twin or helical undulators, or to take beam emittance effects into account, the input can be given as an ASCII-file taken from programs for undulator radiation: *URGENT* [24], *SMUT* [25] or *WAVE* [26]. In this file the intensity and polarisation patterns of the light source must be described as intensity (photons/seconds) and Stokes parameters at a distance of 10 m from the centre of the source in a suitable *x-y* mesh.

Each ray is attributed an energy, E, and a polarisation. The energy can be varied continuously within a 'white' hard-edge band of $E_0 \pm \Delta E$, or toggled between three discrete energies E_0, $E_0 + \Delta E$ and $E_0 - \Delta E$. This feature allows one to determine easily the energy dispersion and the spatial separation of discrete energies for monochromator systems, thereby giving a picture of the energy resolution that one can expect.

Table 2.1 lists the main features of the different light sources.

The source coordinate system for the case of bending magnet synchrotron radiation is given in Fig. 2.3. The storage ring is located in the *x-z* plane,

Table 2.1. Parameters of the *RAY*-sources

	Name	Width x	Height y	Length z	Div. hor. ϕ	Div. vert. ψ	S_0	S_1, S_2, S_3
Matrix	**MA**	Hard	Hard	Hard	Hard	Hard	1	Input
Point	**PO**	Hard soft	Hard soft	Hard	Hard soft	Hard soft	1	Input
Circle	**CI**	Hard	Hard	Hard	Hard	Hard	1	Input
Dipole	**DI**	Soft	Soft	Hard	Hard	Calc.	Flux	Calc.
Wiggler	**WI**	Soft	Soft	$L = n\lambda_{\mathrm{u}}$	Hard	Calc.	Flux	Calc.
Wiggler/Undul.	**WU**	Soft	Soft	0	Calc.	Calc.	Flux	Input
Double–Undul.	**HU**	Soft	Soft	Hard	Soft	Soft	Flux	Input
Undul.–data file	**UF**	Soft	Soft	Hard	File	File	Flux	File
Helical Undul. data file	**HF**	Soft	Soft	Hard	File	File	Flux	File
Source data file	**FI**	Soft	Soft	Hard	File	File	1	Input

hrd, a hard (flat-top) edge; *soft*, soft – a gaussian distribution of the respective variable within a 6σ-width is simulated; *calc*, calculated according to a theoretical model (e.g. Schwinger theory); n, number of wiggler periods; L, length of undulator; λ_{u}, period length; *file*, parameters taken from data-file; *input*, parameters to be given interactively
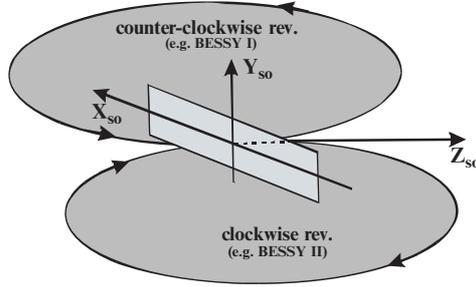
Fig. 2.3. Coordinate system for storage ring-bending magnet sources (*DI_pole*) as viewed from above

PO_int   *PI_xel*   *CI_rcle*
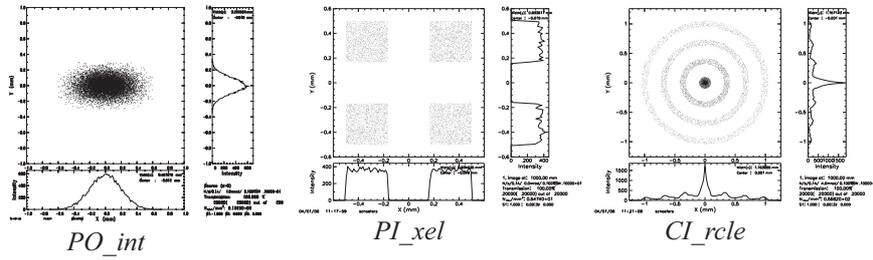
Fig. 2.4. Spot pattern of various source types in x-y plane, projected onto $z = 0$

DI_pole,   *DI_pole,*   *WI_ggler,* seen
Clockwise   Counter-Clockwise   from top
revolution   revolution   (*x-z* plane)
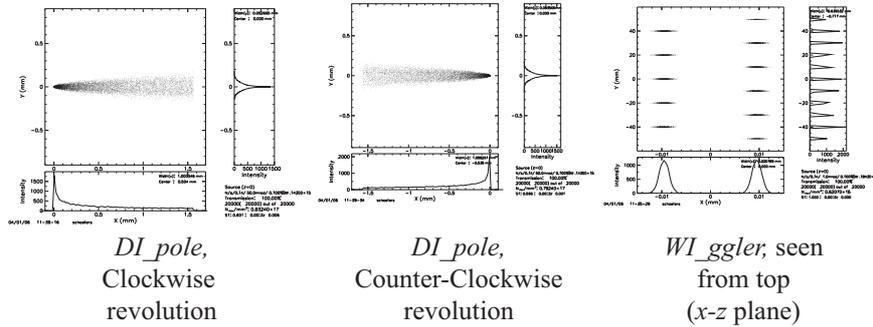
Fig. 2.5. Spot pattern of synchrotron radiation sources in x-y plane, projected onto $z = 0$

for clockwise revolution of the electrons the x-axis is pointing away from the centre, while for counter-clockwise revolution the x-axis is pointing inside the storage ring centre. This is important to be noticed especially for optical systems with large horizontal divergence (e.g. IR-beamlines), where the source cross section is very asymmetric because of the depth-of-field effect (see Fig. 2.5).

Examples of the intensity distribution (footprints) of various sources are given in the Figs. 2.4 and 2.5.

2.5 Interaction of Rays with Optical Elements

2.5.1 Coordinate Systems

The definition of the coordinate system used in RAY is shown in Figs. 2.6 and 2.7. Its origin lies in the centre of the source (with the x-axis in general (e.g. SR) being horizontal). The coordinate system is transformed along the optical path from the source to the optical elements and then to the image planes. The z-axis points into the direction of the central ray, the x-axis is perpendicular to the plane of reflection, i.e. horizontal in the case of a vertically deviating optical setup (azimuthal angles 0° or 180°), and it is vertical for horizontal mounts (azimuthal angles 90° (to the right) and 270° (to the left), respectively). The y-axis is *always* the normal in the centre of the optical element. The plane of reflection or dispersion is, thus, *always* the y-z plane and the surface of the optical elements is the x-z-plane, regardless of the azimuthal angle χ chosen. After the optical element the coordinate system
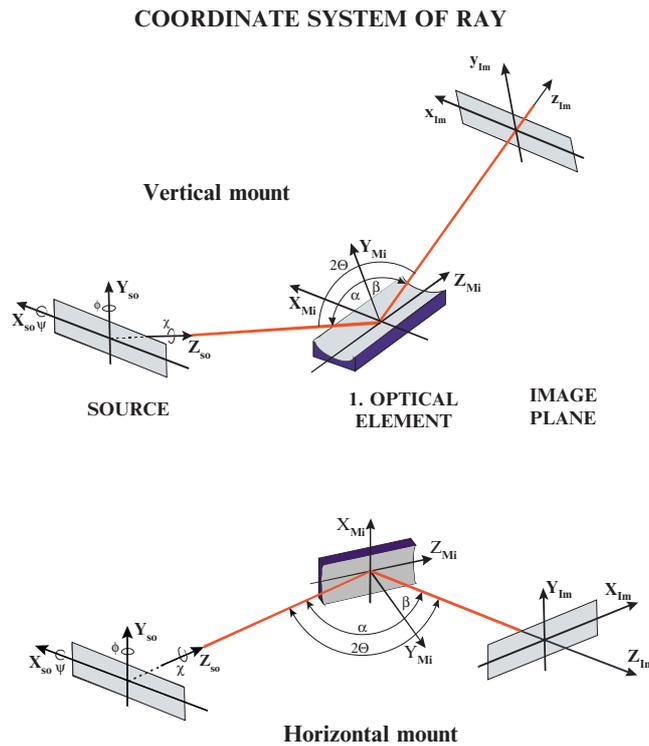
Fig. 2.6. Coordinate system (right-handed screw) and angles used in RAY. (*Top*) Vertical deviation (upwards (downwards)) mount (azimuthal angle $\chi = 0°$ (180°)). (*Bottom*) Horizontal deviation (to the right (left)) (azimuthal angle $\chi = 90°$ (270°)). The optical element is always in the X_M-Z_M-plane
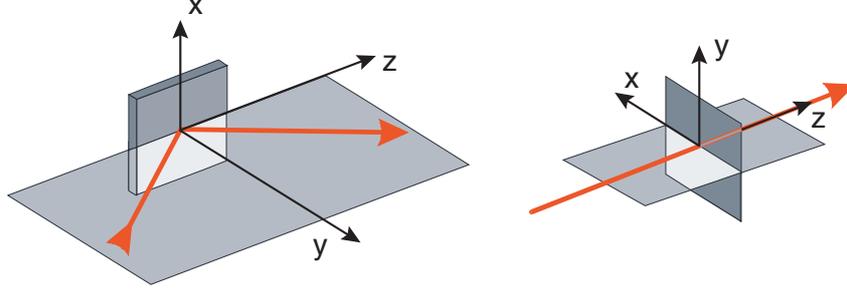
Fig. 2.7. Coordinate systems used in RAY. For optical elements (*left*) the coordinate system is fixed to the optical surface (*X-Z* plane). Transmission elements, screens and image planes (*right*) are in the *X-Y* plane, the *x*-axis is in the horizontal plane. The red line is the light beam

for the outgoing ray is rotated back by $-\chi$, i.e. it has the same orientation as before the optical element. In this way another optical element can be treated in an identical manner.

2.5.2 Geometrical Treatment of Rays

The geometric calculations proceed in the following way:

Statistical creation of a ray within a given source volume and emission cone and within the 'correct' statistics (see Chap. 3). The ray is determined by its source coordinates $(x_{\mathrm{s}}, y_{\mathrm{s}}, z_{\mathrm{s}})$ and its direction cosines $(l_{\mathrm{s}}, m_{\mathrm{s}}, n_{\mathrm{s}})$ determined by the horizontal and vertical emission angles φ and ψ (see Fig. 2.8):

$$\vec{\alpha}_{\mathrm{S}} = \begin{pmatrix} l_{\mathrm{S}} \\ m_{\mathrm{S}} \\ n_{\mathrm{S}} \end{pmatrix} = \begin{pmatrix} \sin\varphi\cos\psi \\ \sin\psi \\ \cos\varphi\cos\psi \end{pmatrix} \tag{2.3}$$

The vector equation of the ray is then

$$\vec{x} = \vec{x}_{\mathrm{S}} + t\vec{\alpha}_{\mathrm{S}} \quad \text{with } t\varepsilon\Re_0^+ \tag{2.4}$$

or, in coordinates

$$\begin{pmatrix} x \\ y \\ z \end{pmatrix} = \begin{pmatrix} x_{\mathrm{s}} \\ y_{\mathrm{s}} \\ z_{\mathrm{s}} \end{pmatrix} + t \begin{pmatrix} l_{\mathrm{S}} \\ m_{\mathrm{S}} \\ n_{\mathrm{S}} \end{pmatrix} \tag{2.5}$$

or

$$\frac{x - x_{\mathrm{s}}}{l_{\mathrm{S}}} = \frac{y - y_{\mathrm{s}}}{m_{\mathrm{S}}} = \frac{z - z_{\mathrm{s}}}{n_{\mathrm{S}}} \tag{2.6}$$
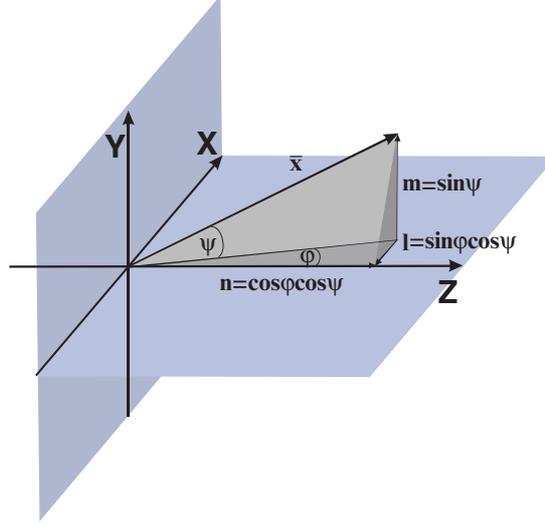
Fig. 2.8. Source coordinate system: Definition of angles and direction cosines in *RAY*

2.5.3 Intersection with Optical Elements

The source coordinate is translated into a new coordinate system with the origin in the centre of the first optical element (hit by the central ray), and the z-axis parallel to a symmetry axis of the optical element (for a simplified equation). The coordinate system is translated by the '*distance from the source*' to the optical element, z_q, rotated around z by the azimuthal angle, χ, and around the new $\tilde{x}$-axis by the grazing incidence angle, θ. The transformation to the new-coordinate system is performed by the following matrix operations:

$$\vec{x}_{S'} = D_{\tilde{x}}(\theta)\, D_z(\chi)\, T_z(z_q)\, \vec{x}_S \tag{2.7}$$

z_q distance source to first optical element or nth to $(n+1)$th element
θ rotation angle around x (y-z plane)
χ azimuthal rotation around z (x-y plane) (clockwise),

which corresponds to

$$\begin{pmatrix} x_{S'} \\ y_{S'} \\ z_{S'} \end{pmatrix} = \begin{pmatrix} 1 & 0 & 0 \\ 0 & \cos\theta & -\sin\theta \\ 0 & \sin\theta & \cos\theta \end{pmatrix} \circ \begin{pmatrix} \cos\chi & -\sin\chi & 0 \\ \sin\chi & \cos\chi & 0 \\ 0 & 0 & 1 \end{pmatrix} \circ \left(\begin{pmatrix} x_S \\ y_S \\ z_S \end{pmatrix} - \begin{pmatrix} 0 \\ 0 \\ z_q \end{pmatrix} \right) \tag{2.8}$$

$$\text{or finally } \begin{pmatrix} x_{S'} \\ y_{S'} \\ z_{S'} \end{pmatrix} = \begin{pmatrix} x_s \cos\chi - y_s \sin\chi \\ x_s \sin\chi \cos\theta + y_s \cos\chi \cos\theta - (z_s - z_q)\sin\theta \\ x_s \sin\chi \sin\theta + y_s \cos\chi \sin\theta + (z_s - z_q)\cos\theta \end{pmatrix} \tag{2.9}$$

The direction cosines are transformed correspondingly:

$$\vec{\alpha}_{S'} = D_{\tilde{x}}(\theta) D_z(\chi) \vec{\alpha}_S, \tag{2.10}$$

$$\text{and finally } \begin{pmatrix} l_{S'} \\ m_{S'} \\ n_{S'} \end{pmatrix} = \begin{pmatrix} l_s \cos\chi - m_s \sin\chi \\ l_s \sin\chi \cos\theta + m_s \cos\chi \cos\theta \\ l_s \sin\chi \sin\theta + m_s \cos\chi \sin\theta \end{pmatrix}. \tag{2.11}$$

In the new coordinate system the ray is described by

$$\begin{pmatrix} x \\ y \\ z \end{pmatrix}(t) = \begin{pmatrix} x_{S'} \\ y_{S'} \\ z_{S'} \end{pmatrix} + t \begin{pmatrix} l_{S'} \\ m_{S'} \\ n_{S'} \end{pmatrix} \tag{2.12}$$

2.5.4 Misalignment

A six-dimensional misalignment of an optical element can be taken into account: three translations of the coordinate system by δx, δy and δz and three rotations by the misorientation angles $\delta\chi$ (x-y plane), $\delta\varphi$ (x-z plane) and $\delta\psi$ (y-z plane). Since the rotations are not commutative, the coordinate system is first rotated by these angles in the given order and then translated. For the outgoing ray to be described in the non-misaligned system, the coordinate system is backtransformed (in reverse order). Thus, the optical axis remains unaffected by the misalignment.

2.5.5 Second-Order Surfaces

Optical elements are described by the general equation for second-order surfaces:

$$\begin{aligned} F(x,y,z) = {}& a_{11}x^2 + a_{22}y^2 + a_{33}z^2 + 2a_{12}xy + 2a_{13}xz \\ & + 2a_{23}yz + 2a_{14}x + 2a_{24}y + 2a_{34}z + a_{44} = 0. \end{aligned} \tag{2.13}$$

This description refers to a right-handed coordinate system attached to the centre of the mirror with its surface in x-z plane, and y-axis points to the normal). This coordinate system is used for the optical elements *PL_ane, CO_ne, CY_linder* and *SP_here*.

Note that for the elements *EL_lipsoid* and *PA_raboloid* a coordinate system is used, which again is attached to the centre of the mirror (with x-axis on the surface), but the z-axis is parallel to the symmetry axis of this element for an easier description in terms of the a_{ij} parameters (see Figs. 2.9 and 2.10). The a_{ij}-values of Table 2.2 are given for this system. Thus, the rotation angle of the coordinate system from source to element is here $\theta + \alpha$ (EL) and 2θ (PA), respectively, θ being the grazing incidence angle and α the tangent angle on the ellipse.
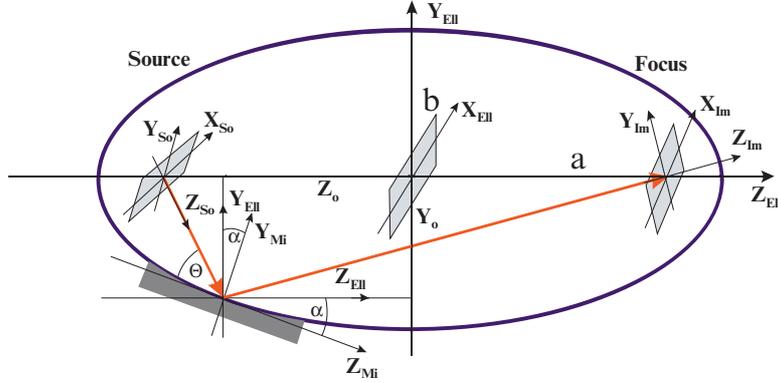
Fig. 2.9. Ellipsoid: definitions and coordinate systems
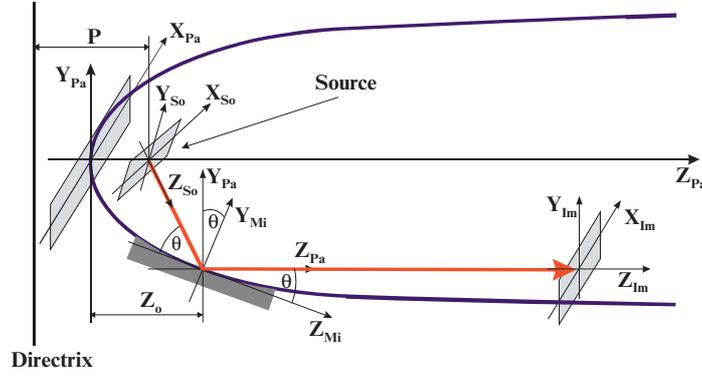
Fig. 2.10. Paraboloid: Definitions and coordinate systems

The individual surfaces are described by the following equations:

- *Plane* $y = 0$
- *Cylinder*(*in z − dir.*) $x^2 + y^2 = 0$
- *Cylinder*(*in x − dir.*) $y^2 + z^2 = 0$
- *Sphere* $x^2 + (y − R)^2 + z^2 − R^2 = 0$
- *Ellipsoid* $x^2/C^2 + (y − y_0)^2/B^2 + (z − z_0)^2/A^2 − 1 = 0$
- *Paraboloid* $x^2/C^2 + (y − y_0)^2/B^2 − 2P(z − z_0) = 0$

$$(2.14)$$

Alternatively to the input of suitable parameters, such as mirror radii or half axes of ellipses, in an experts modus (EO), the a_{ij} parameters can be directly given, such that any second-order surface, whatever shape it has, can be simulated.

Table 2.2. Parameters of the second-order optical elements

Name	PM	CY	CO	SP	EL	PA
a_{11}	0	1/0	$1-c_m$	1	B^2/C^2	P^2/C^2
a_{22}	0	1	$1-2c_m$	1	1	1
a_{33}	0	0/1	0	1	B^2/A^2	0
a_{12}	0	0	0	0	0	0
a_{13}	0	0	0	0	0	0
a_{23}	0	0	$\sqrt{c_m-c_m^2}$	0	0	0
a_{14}	0	0	0	0	0	0
a_{24}	-1	$\rho\cdot sign$	$-a_{23}\dfrac{R}{\sqrt{c_m}}-\dfrac{z_m}{2}$	$R\cdot sign$	$-y_0$	$-y_0$
a_{34}	0	0	0	0	$z_0 B^2/A^2$	$-P$
a_{44}	0	0	0	0	$y_0^2+z_0^2 B^2/A^2 - B^2$	$y_0^2 - 2Pz_0 - P^2$
Sign (concave/convex)	0	1/-1	1/-1	1/-1	1	1
$F_x-(a_{11}x+a_{12}y+a_{13}z+a_{14})$	0	$-x/0$		$-x$	$-a_{11}x$	$-a_{11}x$
$F_y-(a_{22}y\cdot sign+a_{12}x\,a_{23}z+a_{24})$	1	$\rho\cdot sign$		$R\cdot sign$	y_0-y	y_0-y
$F_z-(a_{33}z+a_{13}x+a_{23}y+a_{34})$	0	$0/-z$		$-z$	$-(z_0+z)(B/A)^2$	P
	ρ: radius	ρ: radius	$R,\ \rho$: radii z_m: mirror length $c_m=\left(\dfrac{r-\rho}{z_m}\right)^2$	R: radius	$z_0=A^2/B^2 y_0\tan(\alpha)$ $y_0=r_a\sin(\theta-\alpha)$ $\tan(\alpha)=\tan(\theta)$ $(r_a-r_b)/(r_a+r_b)$	$z_0=f\cos(\alpha,\beta)\cdot sig$ $y_0=f\sin(2\alpha,\beta)$ $P=2f\sin^2(\theta)sig$
					A, B, C half axes in z,y,x-dir; r_a, r_b: mirror to focus 1,2; θ: grazing angle of central ray; α: tangent angle. Plane Ell.: $C=$ infty; Rotational Ell.: $B=C <> A$; Ellipsoid: $A\neq B\neq C$; Sphere: $A=B=C$	f: mirror–source/focus–dist. C: halfpar. in x; Sig $=\pm1$; f: collimation/focussing; θ: grazing angle of central ray; $\alpha,\beta=2\theta,0$ (coll); $\alpha,\beta=0,2\theta$ (foc.). Plane $P:C=$ infty; Rotational $P:C=P$; Elliptical $P:C\neq P$

2.5.6 Higher-Order Surfaces

A similar expert modus is available for surfaces, which cannot be described by the second-order equation. The general equation is the following:

$$\begin{aligned} F(x, y, z) = a_{11}x^2 + \mathrm{sign}a_{22}y^2 + a_{33}z^2 + 2a_{12}xy + 2a_{13}xz + 2a_{23}yz \\ + 2a_{14}x + 2a_{24}y + 2a_{34}z + a_{44} + b_{12}x^2y + b_{21}xy^2 \qquad (2.15) \\ + b_{13}x^2z + b_{31}xz^2 + b_{23}y^2z + b_{32}yz^2 = 0 \end{aligned}$$

Here, again all a_{ij} and b_{ij} parameters can be given explicitly by the user to describe any geometrical surface.

For special higher order surfaces the surface is described by the following equations.

Toroid

$$F(x, y, z) = \left((R - \rho) + \mathrm{sign}\,(\rho)\,\sqrt{\rho^2 - x^2} \right)^2 - (y - R)^2 - z^2 = 0 \qquad (2.16)$$

$$\mathrm{Sign} = \pm 1 \text{ for concave/convex curvature.}$$

The surface normal is calculated according to (see Chap. 5.7)

$$F_x = \frac{-2x\,\mathrm{sign}(\rho)}{\sqrt{\rho^2 - x^2}} \left((R - \rho) + \mathrm{sign}(\rho)\sqrt{\rho^2 - x^2} \right)^2 \qquad (2.17)$$

$$F_y = -2(y - R) \qquad (2.18)$$

$$F_z = -2z. \qquad (2.19)$$

Elliptical Paraboloid

$$F(x, y, z) = \frac{2fx^2}{2f - \frac{z + z_0}{\cos 2\theta}} - 2p(z + z_0) - p^2 = 0. \qquad (2.20)$$

Elliptical Toroid

In analogy to a spherical toroid, an elliptical toroid is constructed from an ellipse (instead of a circle) in the (y, z) plane with small circles of fixed radius ρ attached in each point perpendicular to the guiding ellipse.

The mathematical description of the surface is based on the description of a toroid, where in each point of the ellipse a 'local' toroid with radius $R(z)$ and center $(y_{\mathrm{c}}(z),\ z_{\mathrm{c}}(z))$ is approximated (Fig. 2.11).

Following this description the elliptical toroid surface is given by

$$F(x, y, z) = 0 = (z - z_{\mathrm{c}}\,(z))^2 + (y - y_{\mathrm{c}}\,(z))^2 - \left(R\,(z) - \rho + \sqrt{\rho^2 - x^2} \right)^2$$
$$(2.21)$$
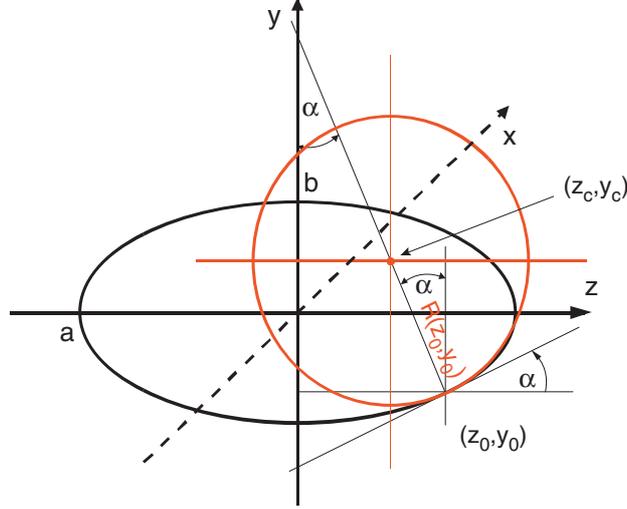
Fig. 2.11. Construction of an elliptical toroid. The ET is locally approximated by a conventional spherical toroid with radius $R(z)$ and center $(z_c(z),\ y_c(z))$

with $R(z) = a^2 b^2 \left(\dfrac{z^2}{a^4} + \dfrac{\left(a^2 - z^2\right)}{a^2 b^2} \right)^{\frac{3}{2}} = \dfrac{1}{ab} \left(\dfrac{b^2 - a^2}{a^2} z^2 + a^2 \right)^{\frac{3}{2}}$

$$z_c(z) = z - R(z)\sin\alpha(z),$$

$$y_c(z) = y(z) + R(z)\cos\alpha(z),$$

$$z_c' = 1 - R'\sin\alpha - R\alpha'\cos\alpha,$$

$$y_c' = y' + R'\cos\alpha - R\alpha'\sin\alpha,$$

$$y(z) = -\frac{b}{a}\sqrt{a^2 - z^2},$$

$$\alpha = \arctan(y') = \arctan\left(\frac{b}{a} \frac{z}{\sqrt{a^2 - z^2}} \right),$$

$$y' = \frac{\partial y}{\partial z} = \tan\alpha = \frac{b}{a}\frac{z}{\sqrt{a^2 - z^2}}$$

$$\alpha' = \frac{\partial\alpha}{\partial z} = \frac{y''}{1 + y'^2},$$

$$y'' = \frac{\partial^2 y}{\partial z^2} = \frac{ab}{\left(a^2 - z^2\right)^{\frac{3}{2}}}.$$

The surface normal is given by the partial derivatives

$$\frac{\partial F}{\partial x} = 2\frac{x}{\sqrt{\rho^2 - x^2}}\left(R - \rho + \sqrt{\rho^2 - x^2} \right), \tag{2.22}$$

$$\frac{\partial F}{\partial y} = 2(y - y_c), \tag{2.23}$$

$$\frac{\partial F}{\partial z} = 2(z - z_c(1 - z_c') - 2y_c'(y - y_c) - 2R'\left(R - \rho + \sqrt{\rho^2 - x^2}\right). \tag{2.24}$$

2.5.7 Intersection Point

The intersection point (x_M, y_M, z_M) of the ray with the optical element is determined by solving the quadratic equation in t generated by inserting (2.12) into (2.13) or (2.15). For the special higher-order surfaces (TO, EP, ET) the intersection point is determined iteratively.

Then the local surface normal for this intersection point $\vec{n} = n(x_M, y_M, z_M)$ is found by calculating the partial derivative of $F(x_M, y_M, z_M)$

$$\vec{f} = \nabla F, \tag{2.25}$$

with the components

$$f_x = \frac{\partial F}{\partial x} \qquad f_y = -\frac{\partial F}{\partial y} \qquad f_z = \frac{\partial F}{\partial z}. \tag{2.26}$$

The local surface normal is then given by the unit vector

$$\vec{n} = \begin{pmatrix} n_x \\ n_y \\ n_z \end{pmatrix} = \frac{1}{\sqrt{f_x{}^2 + f_y{}^2 + f_z{}^2}} \begin{pmatrix} f_x \\ f_y \\ f_z \end{pmatrix}. \tag{2.27}$$

Whenever the intersection point found is outside the given dimensions of the optical element, the ray is thrown away as a geometrical loss and the next ray starts within the source according to Chap. 5.2.

2.5.8 Slope Errors, Surface Profiles

Once the intersection point and the local surface normal is found, these are the parameters that are modified to include real surfaces as deviations from the mathematical surface profile, namely figure and finish errors (slope errors, surface roughness), thermal distortion effects or measured surface profiles.

The surface normal is modified incrementally by rotating the normal vector in the y-z (meridional plane) and in the x-y plane (sagittal). The determination of the rotation angles depends on the type of error to be included.

1. Slope errors, surface roughness: the rotation angles are chosen statistically (according to the procedure described in Sect. 2.3.1) within a 6σ-width of the input value for the slope error.
2. Thermal bumps: a gaussian height profile in x- and z-direction with a given amplitude, and σ-width can be put onto the mirror centre.

3. Cylindrical bending: a cylindrical profile in z-direction (dispersion direction) with a given amplitude can be superimposed onto the mirror surface.
4. Measured surface profiles, e.g. by a profilometer.
5. Surface profiles calculated separately, e.g. by a finite element analysis program.

In cases (2–5) the modified mirror is stored in a 251×251 surface mesh which contains the amplitudes (y-coordinates). For cases (2) and (3) this mesh is calculated within RAY, for the cases (4) and (5) ASCII data files with surface profilometer data (e.g. LTP or ZEISS M400 [27]) or finite-element-analysis data (e.g. ANSYS [28]) can be read in. The new y-coordinate of the intersection point and the local slope are interpolated from such a table accordingly.

2.5.9 Rays Leaving the Optical Element

For those rays that have survived the interaction with the optical element – geometrically and within the reflectivity statistics (Chap. 6) – the direction cosines of the reflected/transmitted/refracted ray $(\vec{\alpha}_2) = (l_2, m_2, n_2)$ are calculated from the incident ray $(\vec{\alpha}_1) = (l_1, m_1, n_1)$ and the local surface normal $\vec{n}$.

Mirrors

For mirrors and crystals the entrance angle, α, is equal to the exit angle, β. In vector notation this means that the cross product is

$$n \times (\vec{\alpha}_2 - \vec{\alpha}_1) = 0, \tag{2.28}$$

since the difference vector is parallel to the normal. For the direction cosines of the reflected ray the result is given by

$$\alpha_2 = \vec{\alpha}_1 - 2(\vec{n} \circ \vec{\alpha}_1)\vec{n} \tag{2.29}$$

or in coordinates

$$l_2 = l_1 - 2n_x \frac{ln_x + mn_y + nn_z}{n_x{}^2 + n_y{}^2 + n_z{}^2} \tag{2.30}$$

and, correspondingly, for m_2 and n_2.

Gratings

The emission angle β for diffraction gratings is obtained by the grating equation

$$k\lambda = d\left(\sin\alpha + \sin\beta\right), \tag{2.31}$$

k, diffraction order; λ, wavelength; d, grating constant.

1. The grating is rotated by $\delta\chi = a\tan(n_x/n_y)$ around the z-axis and by $\delta\psi = a\sin(n_z)$ around the x-axis, so that the intersection point is plane (surface normal parallel to the y-axis). The grating lines are parallel to the x-direction.
2. Then the direction cosines of the diffracted beam are determined by

$$\begin{pmatrix} l_2 \\ m_2 \\ n_2 \end{pmatrix} = \begin{pmatrix} l_1 \\ \sqrt{m_1^2 + n_1^2 - (n_1 - a_1)^2} \\ n_1 - a_1 \end{pmatrix}, \qquad (2.32)$$

$$a_1 = k\frac{\lambda}{d}\cos\delta\psi.$$

3. The grating is rotated back to the original position by $-\delta\psi$ and $-\delta\chi$.

For varied line spacing (VLS) gratings, the local line density $n = 1/d(l/mm)$ as a function of the (x, z)-position is determined by [29]

$$n = n_0 \cdot \left(1 + 2b_2 z + 3b_3 z^2 + 4b_4 z^3 + 2b_5 x + 3b_6 x^2 + 4b_7 x^3\right). \qquad (2.33)$$

Transmitting Optics

For transmitting optics (*SL_it, FO_il*) the direction of the ray is unchanged by geometry. However, diffraction is taken into account for the case of rectangular or circular slits by randomly modifying the direction of each ray according to the probability for a certain direction φ

$$P(\varphi) = \frac{\sin u}{u}, \qquad (2.34)$$

$$\text{with } u = \frac{\pi b \sin\varphi}{\lambda}(b, \text{ slit opening}; \lambda, \text{ wavelength}),$$

so that for a statistical ensemble of rays a Fraunhofer (rectangular slits) or bessel pattern (circular slits) appears (see Fig. 2.12). *ZO_neplate* transmitting optics are described in [12, 13].

Azimuthal Rotation

After successful interaction with the optical element the surviving ray is described in a coordinate system, which is rotated by the reflection angle θ and the azimuthal angle χ, such that the z-axis follows once again the direction of the outgoing central ray as it was for the incident ray. The old values of the source/mirror points and direction cosines are replaced by these new ones, so that a new optical element can be attached now in similar way.
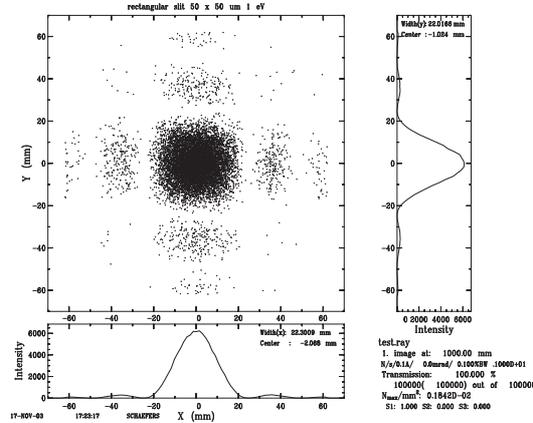
Fig. 2.12. Fraunhofer diffraction pattern on a rectangular slit

2.5.10 Image Planes

If the ray has traversed the entire optical system, the intersection points $(x_I,\ y_I)$ with up to three image planes at the distances $z_{I_{1,2,3}}$ are determined according to

$$\begin{pmatrix} x_I \\ y_I \end{pmatrix} = \begin{pmatrix} x \\ y \end{pmatrix} + \frac{1}{n} \begin{pmatrix} l \\ m \end{pmatrix} (z_{I_{1,2,3}} - z).$$ (2.35)

Once a ray reaches the image plane or whenever a ray is lost within the optical system a new ray is created within the source and the procedure starts all over.

2.5.11 Determination of Focus Position

For the case of imaging systems, if the focus position is to be determined, the x- and y-coordinates of that ray which has the largest coordinates are stored along the light beam in the range of the expected focal position (*search in a distance from last OE of* $\ldots +/- \ldots$). The so found cross section of the beam (width and height) is displayed graphically. Since at each position a different ray may be the outermost one, there may be bumps in this focal curve which depend on the quality of the imaging. Especially, for optical systems with large divergences (and thus large optical aberrations) or which include dispersing elements, this curve is only schematic and serves as a quick check of the focal properties of the system.

2.5.12 Data Evaluation, Storage and Display

The x, z-coordinates of the intersection point (x, y for source, slits, foils, zoneplates and image planes) and the angles l, n (l, m, respectively) are stored into 100×100 matrices. These matrices are multichannel arrays, one for the source, for each optical element and for each image plane, whose dimensions

(and with it the pixel size) have been fixed before in a 'test-raytrace' run. They represent the illuminated surface in x-z projection. The corresponding surface pixel element that has been hit by a ray is increased by 1, so that intensity profiles and/or heat load can be displayed.

Additionally, the x- and z-coordinates (y, respectively) of the first 10,000 rays are stored in a 10,000x2 ASCII matrix to display footprint patterns of the optical elements, for point diagrams at the image planes or for further evaluation outside the program.

2.6 Reflectivity and Polarisation

Not only the geometrical path of the rays is followed, but also the intensity and polarisation properties of each ray are traced throughout an optical setup. Thus, it is easily possible to preview depolarisation effects throughout the optical path, or to optimize an optical setup for use as, for example, a polarisation monitor. For this, each ray is treated individually with a defined energy and polarisation state.

RAY employs the Stokes formalism for this purpose. The Stokes vector $\vec{S} = (S_0, \ S_1, \ S_2, \ S_3)$ describing the polarisation (S_1, S_2: linear, S_3: circular polarisation) for each ray is given either as free input parameter or, for dipole sources, is calculated according to the Schwinger theory. S_0, the start intensity of the ray from the source $\left(S_0 = \sqrt{S_1{}^2 + S_2{}^2 + S_3{}^2}\right)$, is set to 1 for the artificial sources. It is scaled to a realistic photon flux value for the synchrotron sources Dipole, Wiggler or the Undulator-File.

The Stokes vector is defined by the following equations:

$$
\begin{aligned}
S_0 &= \left[(E^{\mathrm{o}}{}_{\mathrm{p}})^2 + (E^{\mathrm{o}}{}_{\mathrm{s}})^2\right]\Big/2 = 1, \\
S_1 &= \left[(E^{\mathrm{o}}{}_{\mathrm{p}})^2 - (E^{\mathrm{o}}{}_{\mathrm{s}})^2\right]\Big/2 = P_{\mathrm{l}}\cos(2\delta), \\
S_2 &= E^{\mathrm{o}}{}_{\mathrm{p}}E^{\mathrm{o}}{}_{\mathrm{s}}\cos(\phi_{\mathrm{p}} - \phi_{\mathrm{s}}) = P_{\mathrm{l}}\sin(2\delta), \\
S_3 &= -E^{\mathrm{o}}{}_{\mathrm{p}}E^{\mathrm{o}}{}_{\mathrm{s}}\sin(\phi_{\mathrm{p}} - \phi_{\mathrm{s}}) = P_{\mathrm{c}},
\end{aligned}
\tag{2.36}
$$

with the two components of the electric field vector defined as

$$
E_{\mathrm{p,s}}(z,t) = E^{\mathrm{o}}_{\mathrm{p,s}}\exp\left[\mathrm{i}\left(\omega t - kz + \phi_{\mathrm{p,s}}\right)\right].
\tag{2.37}
$$

and P_{l}, P_{c} are the degree of linear and circular polarisation, respectively. δ is the azimuthal angle of the major axis of the polarisation ellipse. Note that

$$
\begin{aligned}
P_{\mathrm{l}} &= P\cos(2\varepsilon) \\
\text{and} \quad P_{\mathrm{c}} &= P\sin(2\varepsilon),
\end{aligned}
\tag{2.38}
$$

with P being the degree of total polarisation and ε the ellipticity of the polarisation ellipse $(\tan\varepsilon = R_{\mathrm{p}}/R_{\mathrm{s}})$.

Table 2.3. Definition of circular polarisation

Phase $\phi_{\mathrm{p-s}}$	90°, −270° $(\pi/2, -3\pi/2)$	−90°, 270° $(-\pi/2, 3\pi/2)$
Rotation sense (in time)	Clockwise	Counter-clockwise
Rotation sense (in space)	Counter-clockwise	Clockwise
Polarisation (optical def.)	R(ight) CP	L(eft) CP
Helicity (atomic def.)	Negative $(\sigma-)$	Positive $(\sigma+)$
Stokes vector	Negative	Positive

Table 2.4. Physical interaction for the different optical components

Mirrors	Gratings	Foils	Slits	Zone-plates	Crystals
Fresnel equations	Diffraction	Fresnel equations	–	–	Dynamic theory
Reflectivity	Efficiency	Transmission	Transmission	Transmission	Reflectivity
$R_{\mathrm{s}}, R_{\mathrm{p}}, \Delta_{\mathrm{sp}}$	$E_{\mathrm{s}}, E_{\mathrm{p}}, \Delta_{\mathrm{sp}}$	$T_{\mathrm{s}}, T_{\mathrm{p}}, \Delta_{\mathrm{sp}}$	$T_{\mathrm{s}}, T_{\mathrm{p}} = 1$ $\Delta_{\mathrm{sp}} = 0$	$T_{\mathrm{s}}, T_{\mathrm{p}} = 1,$ $\Delta_{\mathrm{sp}} = 0$	$R_{\mathrm{s}}, R_{\mathrm{p}}, \Delta_{\mathrm{sp}}$

Since the SR is linearly polarised within the electron orbital plane ($I_{\mathrm{perp}} = 0$), the plane of linear polarisation is coupled to the x-axis (i.e. horizontal). Thus, the Stokes vector for SR is defined in our geometry as (see Chap. 3.4)

$$P_{\mathrm{lin}} = S_1 = (I_{\mathrm{perp}} - I_{\mathrm{par}})/(I_{\mathrm{perp}} + I_{\mathrm{par}}) = (I_y - I_x)/(I_y + I_x) = -1, \quad (2.39)$$

$S_1 = +1$ would correspond to a vertical polarisation plane.

For the definition of the circular polarisation the nomenclature of Westerfeld et al. [30] and Klein/Furtak [31] has been used. This is summarised in Table 2.3:

For example, for the case of synchrotrons and storage rings, the radiation that is emitted off-plane, upwards, has negative helicity, right-handed CP ($S_3 = -1$), when the electrons are travelling clockwise, as seen from the top.

The modification of the Stokes vector throughout the beamline by interaction of the light with the optical surface is described by the following steps (see e.g. [28]):

(1) Give each ray a start value for the Stokes parameter within the source, S_{ini}, according to input or as calculated for SR sources
(2) Calculate the intensity loss at the first optical element for s- and p-polarisation geometry and the relative phase, $\Delta = \delta_{\mathrm{s}} - \delta_{\mathrm{p}}$, according to the physical process involved (see Table 2.4):
   • Mirrors, Foils
   The optical properties of mirrors, multilayers, filters, gratings and crystals are calculated from the compilation of atomic scattering factors in the spectral range from 30 eV to 30 keV [32]. Another data set covers the X-ray range from 5 up to 50 keV [33]. Additional data for lower energies down to 1 eV are also available for some elements and molecules [34].

Optical data tables for RAY

Molecules: Al_2O_3, MgF_2, Diamond, SiC, SiO_2...n,k

Palik (Al, Au, C, Cr, Cu, Ir, Ni, Os, Pt, Si... n, k)

Henke (Z=1-92) f_1, f_2

Cromer f_1,f_2
(Z=2-92)

Structure factors f_o, f_H, f_{HC}

10^{-3}	10^{-2}	10^{-1}	10^0	10^1	10^2

Photon Energy (keV)
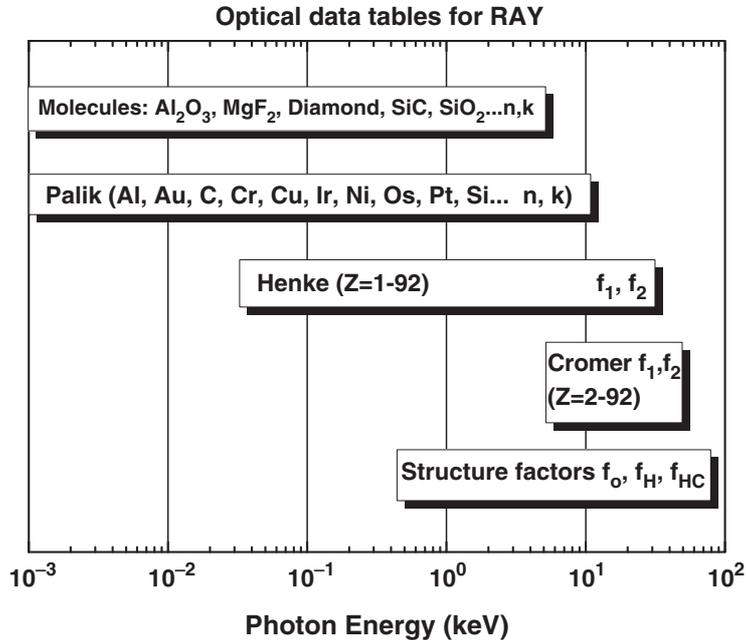
Fig. 2.13. Data bases used for the calculation of optical properties

A summary of the various data tables available within the program is given in Fig. 2.13. For compound materials that can be defined by the case sensitive chemical formula (e.g. MgF_2), the contributions of the chemical elements are weighted according to their stochiometry. A tabulated or, if not available, calculated value for the density is proposed but can be changed. The surface roughness of mirrors or multilayers is taken into account according to the Nevot–Croce formalism [35].

All reflection mirrors and transmission foils in an optical setup can have a multilayer coating (plus an additional top coating). The optical properties of these structures are calculated in transmission and reflection geometry by a recursive application of the Fresnel equations. For periodic multilayers, the layer thickness, the density and the surface roughness must be specified for each type of interface. For aperiodic structures like broad-band or supermirrors, the exact structure has to be provided in a data-file.

• Gratings

For the calculation of (monolayer covered) reflection gratings, a code developed by Neviere is used [36], which allows for the calculation for three different grating profiles (sinusoidal, laminar or blazed). In addition to fixed deviation angle mounts, optionally the incidence angle can be coupled to the photon energy and the c_{ff} factor in the case of a Petersen

SX700 type monochromator (PGM or SGM with a plane pre-mirror which enables the deviation angle across the grating to be varied).

- Crystals

For crystals the diffraction properties are calculated from the dynamical theory using the Darwin–Prins formalism [37]. For all crystals with zinc blende structure such as Si, Ge or InSb as well as for quartz and beryl, the crystal structure factors are determined within the program for any photon energy and the corresponding Bragg angle. For other crystals, the rocking curves can also be evaluated if the structure factors are known from other sources. The calculation is possible for any allowed crystal reflection and asymmetry (see Chap. 2.7).

(3) Transform the incident Stokes vector, $\vec{S}_{\text{ini}}$, into the coordinate system of the optical element $\vec{S}_{\text{M}}$ by rotation around the azimuthal angle χ (R-matrix)

$$\vec{S}_{\text{M}} = R_{\tilde{y}}(\chi)\vec{S}_{\text{ini}}, \tag{2.40}$$

$$\vec{S}_{\text{M}} = \begin{pmatrix} S_{0\text{M}} \\ S_{1\text{M}} \\ S_{2\text{M}} \\ S_{3\text{M}} \end{pmatrix} = \begin{pmatrix} 1 & 0 & 0 & 0 \\ 0 & \cos 2\chi & \sin 2\chi & 0 \\ 0 & -\sin 2\chi & \cos 2\chi & 0 \\ 0 & 0 & 0 & 1 \end{pmatrix} \bullet \begin{pmatrix} S_{0\text{ini}} \\ S_{1\text{ini}} \\ S_{2\text{ini}} \\ S_{3\text{ini}} \end{pmatrix}. \tag{2.41}$$

Thus, the azimuthal angle of an optical element determines the polarisation geometry of the interaction. For instance, for horizontally polarised synchrotron radiation ($S_1 = -1$), an azimuthal angle of $\chi = 0°$ corresponds to an s-polarisation geometry (polarisation plane perpendicular to the reflection plane) with the beam going upwards. Since the coordinate system is right-handed, $\chi = 90°$ corresponds to a deviation to the right, when looking with the beam and a p-polarisation geometry (polarisation plane parallel to reflection plane). Similarly $\chi = 180°$ and $270°$, respectively, determine a beam going down and to the left, respectively. Note that the azimuthal angle is coupled to the coordinate system and not to the polarisation state. $\chi = 0°$ always determines a deviation upwards, but this may be an s-polarisation geometry, as in our example above, and can also be a p-geometry (when $S_{1\text{inc}} = +1$).

(4) Calculate the Stokes vector after the optical element $\vec{S}_{\text{final}}$ by applying the Müller matrix, M, onto $\vec{S}_{\text{M}}$

$$\vec{S}_{\text{final}} = M\vec{S}_{\text{M}} \tag{2.42}$$

$$\begin{pmatrix} S_{0\text{final}} \\ S_{1\text{final}} \\ S_{2\text{final}} \\ S_{3\text{final}} \end{pmatrix} = \begin{pmatrix} \frac{R_{\text{s}}+R_{\text{p}}}{2} & \frac{R_{\text{p}}-R_{\text{s}}}{2} & 0 & 0 \\ \frac{R_{\text{p}}-R_{\text{s}}}{2} & \frac{R_{\text{s}}+R_{\text{p}}}{2} & 0 & 0 \\ 0 & 0 & R_{\text{s}}R_{\text{p}}\cos\Delta & R_{\text{s}}R_{\text{p}}\sin\Delta \\ 0 & 0 & -R_{\text{s}}R_{\text{p}}\sin\Delta & R_{\text{s}}R_{\text{p}}\cos\Delta \end{pmatrix} \circ \begin{pmatrix} S_{0\text{M}} \\ S_{1\text{M}} \\ S_{2\text{M}} \\ S_{3\text{M}} \end{pmatrix}. \tag{2.43}$$

(5) Accept this ray only when its intensity ($S_{0,\text{final}}$) is within the 'correct' statistic, i.e. when

$$(S_{0,\text{final}}/S_{0,\text{ini}} - ran\,(z)) > 0. \qquad (2.44)$$

(6) Rotate the Stokes vector $\vec{S}_{\text{final}}$ back by $-\chi$ and take this as incident Stokes vector for the next optical element

$$\vec{S}'_{\text{ini}} = R_{\tilde{y}}(-\chi)\vec{S}_{\text{final}}. \qquad (2.45)$$

(7) Store the Stokes vector for this optical element, go to the next one (2) or start with the next ray within the source (1).

2.7 Crystal Optics (with M. Krumrey)

For ray tracing, the geometrical point of view is most relevant. In this aspect, the main difference between crystals and mirrors or reflection grating is that the radiation is not reflected at the surface, but at the lattice planes in the material. In contrast to gratings which have already been treated as dispersive elements, reflection for a given incidence angle on the lattice plane occurs only if the well-known Bragg condition is fulfilled:

$$\lambda = 2d\sin\Theta, \qquad (2.46)$$

where λ is the wavelength, d is the lattice plane distance and Θ is the incidence angle of the radiation with respect to the lattice plane. The selected lattice planes are not necessarily parallel to the surface, resulting in an asymmetry described by the asymmetry factor b:

$$b = \frac{\sin(\theta_{\text{B}} - \alpha)}{\sin(\theta_{\text{B}} + \alpha)}, \qquad (2.47)$$

with Θ_{B} being the Bragg angle for which (2.46) is fulfilled and α the angle between the lattice plane and the crystal surface.

The subroutine package for crystal optics in RAY is based on the description of dynamic theory [38–40] as given by Matsushita and Hashizume in [41] and the paper from Batterman and Cole [37]. The reflectance is calculated according to the Darwin–Prins formalism, which requires the knowledge of the crystal structure factors F_{o}, F_{h} and F_{hc}. These factors can be derived for any desired crystal reflection, identified by the Miller indices (hkl), if the crystal structure, the chemical elements involved and the lattice constants (or constants for non-cubic crystals) are known. For some crystals with zinc blende structure (e.g. Si, InSb, etc.) or quartz structure, the structure factors are calculated automatically. This calculation combines the geometrical properties, especially the atomic positions in the unit cell which are read from a

file, with the element-specific atomic scattering factors. The atomic scattering factor, f, is written here as

$$f = f_0 + \Delta f_1 + \Delta f_2. \tag{2.48}$$

This form allows one to separate the form factor f_0, which is calculated in dependence on $(\sin \theta_B)/\lambda$ based on a table of nine coefficients which are read for every chemical element from a file. The photon energy dependent anomalous dispersion corrections Δf_1 and Δf_2 are calculated from the Henke tables for photon energies up to 30 keV. For higher photon energies, the Cromer tables are directly used up to 50 keV and extrapolated beyond. Both data sets are also stored in files for all chemical elements.

Using the structure factors F_o, F_h and F_{hc}, which can, for other crystals, also be inserted by the user, the reflectance is obtained as

$$R = (\eta \pm \sqrt{\eta^2 - 1})s. \tag{2.49}$$

Here, s is simply defined as

$$s = \sqrt{F_h / F_{hc}} \tag{2.50}$$

while the parameter η is calculated according to

$$\eta = \frac{2b(\alpha - \Theta_B) \sin 2\Theta + \gamma F_o(1 - b)}{2\gamma |P| s \sqrt{|b|}}, \tag{2.51}$$

where γ is defined as

$$\gamma = \frac{r_e \lambda^2}{\pi V_C}. \tag{2.52}$$

Here, r_e is the classical electron radius and V_c is the crystal unit cell volume. The polarisation is taken into account by the factor P, which equals unity for σ-polarisation and $\cos 2\Theta_B$ for π-polarisation.

In addition to the reflectance, the dispersion correction $\Delta\Theta$ for the incident and the outgoing ray at the crystal surface is calculated. For this purpose a crystal reflection curve is calculated according to (2.49) and the difference from its centre to the Bragg angle Θ_B is extracted. Only in the case of symmetrically cut crystals are the dispersion corrections identical:

$$\Delta\Theta_{out} = b\Delta\Theta_{in}. \tag{2.53}$$

At present, plane and cylindrical crystals are treated in reflection geometry (Bragg case). Also crystals with a d-spacing gradient (graded crystals with $d = d(z)$) are taken into account. This versatility enables a realistic simulation to be made of nearly every X-ray-optical arrangement in use with conventional X-ray sources or at synchrotron radiation facilities (double-, four
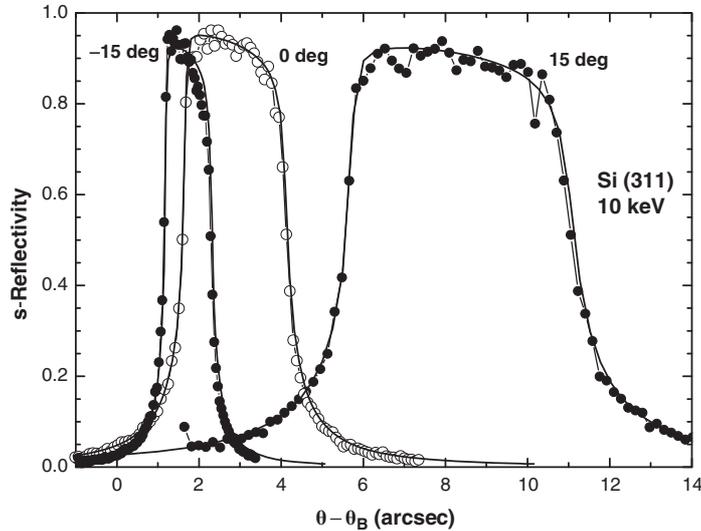
Fig. 2.14. Rocking curves of Si(311) crystal with asymmetric cut ($15°$ and $-15°$) and symmetric cut ($0°$) for σ-polarisation at a photon energy of $10\,\text{keV}$

crystal monochromators, 2-bounce, 4-bounce in-line geometries for highest resolution, dispersive or non-dispersive settings, etc. [42,43]).

Typical X-ray reflectance curves obtained with this subroutine package are shown for illustration. The raytracing code was applied for the calculations of Si(311) asymmetrically and symmetrically cut flat crystals. The angle of asymmetry was chosen to be $15°$ and $-15°$. In Fig. 2.14 the comparative results between *RAY* and *REFLEC* [12] codes for the σ-polarisation state are shown. *RAY* results in this figure are represented by the noisy curve. The statistics are determined by the number of rays calculated (10^6 incident rays, distributed into 100 channels).

2.8 Outlook: Time Evolution of Rays (with R. Follath, T. Zeschke)

In this article a program has been described, which is capable of simulating the behaviour of an optical system. Originally the program was designed for the calculation of X-ray optical setups on electron storage rings for synchrotron radiation. Similar programs had been written at most of the facilities for in-house use tailored to their specific applications. Many of them have not survived. Over more than 20 years of use by many people and continuous upgrade, debugging and development, the RAY-program described here has turned into a versatile optics database, by which almost all of the existing synchrotron radiation beamlines from the infrared region to the hard X-ray range can be accessed. In addition, other sources can be modelled since the light sources are described by relatively few parameters.

However, the program has limitations, of course, and it is essential to be aware of them when using it:

- The results are valid only within the mathematical or physical model implemented.
- The program may still have bugs (it has – definitely!!).
- The user may have made typing errors in the input menu.
- The user may have made errors in interpreting unclear or ambiguous input parameters or results.

The program is in continuous development and new ideas about sources or optical elements are implemented relatively fast, so that new demands can be addressed quickly.

One of the latest developments was driven by the advent of the new generation Free Electron Light (FEL) Sources at which the time structure of the radiation in the femto-second regime is of utmost importance. As outlook for the future of raytracing this development, which is still in progress, is discussed here briefly.

To handle the time structure, a ray is not only described by its geometry, energy and polarisation, but also by its geometrical path length or, in other words, by its travel time.

This enables one to follow the time evolution of an ensemble of rays, starting with a well-defined time-structure in the source, through an optical system. By storing the individual path lengths of each ray a pulse-broadening at each element and at the focal plane can be detected.

In the source, each ray is given a start-clock time, t_0, which can be either $t_0 = 0$ for all rays (complete coherence), or have a gaussian or flat-top distribution (less than complete coherence).

The path length of a ray is calculated as difference between the coordinates of the previous optical element (*x_old, y_old, z_old*) (or, for the first optical element, the source coordinates (*x_so, y_so, z_so*)) and the actual coordinates (*x,y,z*). The path length is measured with respect to the path length of the principal ray, given by the *distance to the preceding element zq*. Only geometrical differences are taken into account, no phase changes on reflection or penetration effects on multilayers are considered.

The path length is given by the equation

$$\mathrm{pl} = \sqrt{((x - x_{\mathrm{old}})^2 + (y - y_{\mathrm{old}})^2 + (z - z_{\mathrm{old}})^2)} - zq. \qquad (2.54)$$

The phase of the ray with respect to the central ray and its relative travel time is then

$$\varphi = \frac{2\pi}{\lambda}\mathrm{pl}, \qquad (2.55)$$

$$t = \frac{\mathrm{pl}}{c} \qquad c\text{: speed of light (m s}^{-1}\text{)}. \qquad (2.56)$$

Assuming pl in millimetre, the travel time is given in nanoseconds.
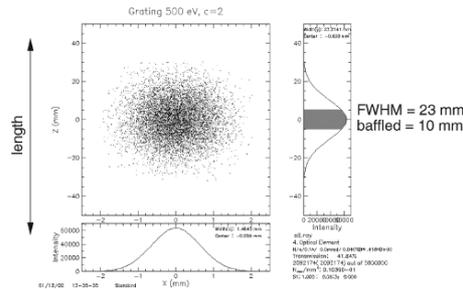
Fig. 2.15. Illumination of a reflection grating and baffling to preserve the time structure of the light beam
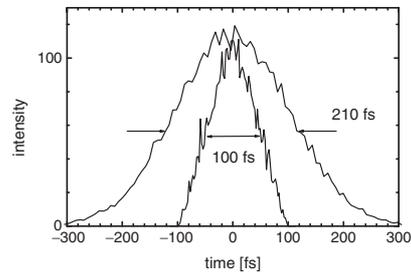
Fig. 2.16. Time structure of the rays after travelling through the beamline; confined–unconfined by the grating of Fig. 2.15

As an example, Fig. 2.15 shows the illumination of a reflection grating, which is part of a soft X-ray plane grating monochromator (PGM-) beamline that has been modelled for the TESLA FEL project [44], in which the conservation of the fs-time structure is essential. By baffling the illuminated grating length down to 10 mm in the dispersion direction the pulse broadening of the monochromatic beam (Fig. 2.16) can be kept well within the required 100 fs, which corresponds to the time structure of a SASE-FEL-source. As a result, the pulse length remains essentially unchanged by the optics.

By combining the path length information of each ray with its spatial information (footprint on an optical element or focus) a three-dimensional space–time picture over an ensemble of rays can be constructed. Such an example is given in Fig. 2.17. Here the focus of a highly demagnifying toroidal mirror (10:1) illuminated at grazing incidence (2.5°) by a diffraction-limited gaussian source with $\sigma = 0.2$ mm cross section and $\sigma = 0.3$ mrad divergence is shown. The illumination is coherent, i.e. all rays have the same start-time within the source. The focus (Fig. 2.17a) shows the typical blurring due to coma and astigmatic coma, and the grey scale colour attributed to each ray (Fig. 2.17b) determines the relative travel time (i.e. phase) with respect to the central ray. This is a snap shop over the focus; rays arrive at the focus in a time indicated by an increasing grey-scale.
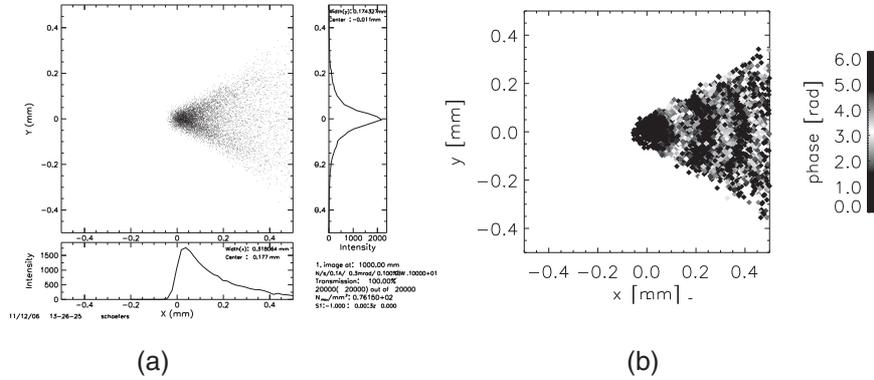
Fig. 2.17. Footprint of rays (**a**) and their individual phases (**b**) arriving at the focus of a toroidal mirror in grazing incidence ($\theta = 2.5°$, 10:1 demagnification)
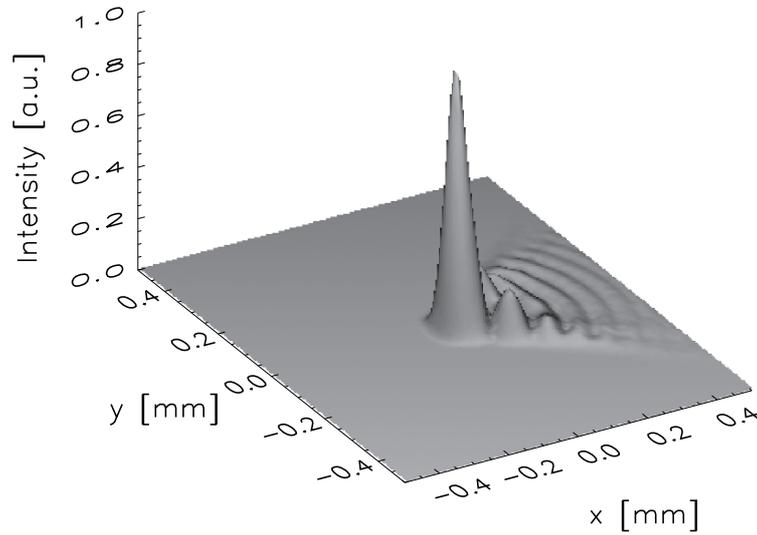
Fig. 2.18. Interference pattern at the focus of a 2.5° incidence toroidal mirror, 10:1 demagnification

In the individual phases an interference pattern in the coma blurred wings becomes visible. After complex addition of all rays within a certain array element according to

$$I = \left| \sum_j e^{i\varphi_j} \right|^2 , \tag{2.57}$$

an interference pattern becomes visible also in the intensity profile (Fig. 2.18). This profile looks very similar to the results obtained with programs on

the basis of Fourier-Optics (see this book [6]) and shows the potential of a conventional raytrace program in treating interference effects.

So far in this simple example only the phase and the space coordinates of the rays have been connected to demonstrate the treatment of collective interference effects in the particle model. This model can be extended further to incoherent or partially coherent illumination simply by modifying the incident time-variable of the source suitably. Coherent packages within a total ensemble of rays can be extracted, which are determined by the same wavelength, the same polarisation plane, the same x-y-position (lateral coherence length) or the same path length (transversal coherence). Hence, there is a huge potential for further development of wave-phenomena within the particle model.

Acknowledgements

References

1. J. Feldhaus, *RAY* (unpublished) and personal communication (1984)
2. C. Welnak, G.J. Chen, F. Cerrina, Nucl. Instrum. Methods Phys. Res. A **347**, 344 (1994)
3. T. Yamada, N. Kawada, M. Doi, T. Shoji, N. Tsuruoka, H. Iwasaki, J. Synchrotron Radiat. **8**, 1047 (2001)
4. J. Bahrdt, Appl. Opt. **36**, 4367 (1997)
5. O. Chubar, P. Elleaume, in *Proceedings of 6th European Particle Accelerator Conference EPAC-98*, 1998, pp. 1177–1179
6. M. Bolder, J. Bahrdt, O. Chubar, *Wavefront Propagation* (this book, Chapter 5)
7. P.R. Bevington, *Data Reduction and Error Analysis for the Physical Sciences* (McGraw-Hill, New York, 1969)
8. M. Born, E. Wolf, *Principles of Optics*, 6th edn. (Pergamon Press, New York, 1980)

9. F.A. Jenkins, H.E. White, *Fundamentals of Optics*, 4th edn. (McGraw-Hill, New York, 1981)
10. W.B. Peatman, *Gratings, Mirrors and Slits* (Gordon & Breach, New York, 1997)
11. A. Pimpale, F. Schäfers, A. Erko, Technischer Bericht, BESSY **TB 190**, 1 (1994)
12. A. Erko, F. Schäfers, N. Artemiev, in *Advances in Computational Methods for X-Ray and Neutron Optics SPIE-Proceedings*, vol. 5536, 2004, pp. 61–70
13. A. Erko, in *X-Ray Optics; Raytracing model of a Zoneplate*, ed. by B. Beckhoff et al. Handbook of Practical X-Ray Fluorescence Analysis (Springer, Berlin Heidelberg New York, 2006) pp. 173–179
14. F. Schäfers, Technischer Bericht, BESSY **TB 202**, 1 (1996)
15. F. Schäfers and M. Krumrey, Technischer Bericht, BESSY **TB 201**, 1 (1996)
16. H. Petersen, C. Jung, C. Hellwig, W.B. Peatman, W. Gudat, Rev. Sci. Instrum. **66**, 1 (1995)
17. W.B. Peatman, U. Schade, Rev. Sci. Instrum. **72**, 1620 (2001)
18. M.R. Weiss, et al. Nucl. Instrum. Methods Phys. Res. A **467–468**, 449 (2001)
19. A. Erko, F. Schäfers, W. Gudat, N.V. Abrosimov, S.N. Rossolenko, V. Alex, S. Groth, W. Schröder, Nucl. Instrum. Methods Phys. Res. A **374**, 408 (1996)
20. A. Erko, F. Schäfers, A. Firsov, W.B. Peatman, W. Eberhardt, R. Signorato Spectrochim. Acta B **59**, 1543 (2004)
21. *EFFI: Software Code to Calculate VUV/X-ray Optical Elements*, developed by F. Schäfers, BESSY, Berlin (unpublished)
22. *OPTIMO: Software Code to Optimize VUV/X-ray Optical Elements*, developed by F. Eggenstein, BESSY, Berlin (unpublished)
23. J. Schwinger, Phys. Rev. **75**, 1912 (1949)
24. *URGENT: Software Code for Insertion Devices*, developed by R.P. Walker, B. Diviacco, Sincrotrone Trieste, Italy (1990)
25. C. Jacobson, H. Rarback, in *Insertion Devices for Synchrotron Radiation*. SPIE Proc., vol. 582 (*SMUT: Software code for insertion devices*), 1985, p. 201
26. *WAVE: Software Code for Insertion Devices*, developed by M. Scheer, BESSY, Berlin (unpublished)
27. *M400: Coordinate Measuring Machine*, ZEISS, Oberkochen, Germany
28. *ANSYS: Finite Element Analysis (FEM) Program*, registered trademark of SWANSON Analyzer Systems, Inc., Houston, TX
29. M. Fujisawa, A. Harasawa, A. Agui, M. Watanabe, A. Kakizaki, S. Shin, T. Ishii, T. Kita, T. Harada, Y. Saitoh, S. Suga, Rev. Sci. Instrum. **67**, 345 (1996)
30. W.B. Westerveld, K. Becker, P.W. Zetner, J.J. Corr, J.W. McConkey, Appl. Opt. **24**, 2256 (1985)
31. M.V. Klein, T.E. Furtak, *Optik* (Springer-Lehrbuch, Berlin Heidelberg New York, 1988)
32. B.L. Henke, E.M. Gullikson, J.C. Davis, At. Data Nucl. Data Tables **54**, 181 (1993)
33. D.T. Cromer, J.T. Waber, *Atomic Scattering Factors for X-Rays in International Tables for X-Ray Crystallography*, vol. IV (Kynoch Press, Birmingham, 1974), pp. 71–147
34. E.D. Palik (ed.), *Handbook of Optical Constants of Solids* (Academic Press, New York, 1985); J.H. Weaver et al., Phys. Data **18**, 2 (1981)
35. L. Nevot, P. Croce, Rev. Phys. Appl. **15**, 761 (1980)
36. M. Neviere, J. Flamand, J.M. Lerner, Nucl. Instrum. Methods **195**, 183 (1982); R. Petit (ed.) *Electromagnetic Theory of Gratings*, (Springer Verlag, Berlin Heidelberg New York, 1980) and references therein

37. B.W. Batterman, H. Cole, Rev. Mod. Phys. **36**, 681 (1964)
38. D.W.J. Cruickshank, H.J. Juretsche, N. Kato (eds.), *P.P. Ewald and his Dynamical Theory of X-ray Diffraction* (International Union of Crystallography and Oxford University Press, Oxford, 1992)
39. W.H. Zachariasen, *Theory of X-ray Diffraction in Crystals*, (Wiley, New York, 1945)
40. Z.G. Pinsker, *Dynamical Scattering of X-rays in Crystals*, (Springer Verlag, Berlin Heidelberg New York, 1978)
41. T. Matsushita, H. Hashizume, In: *Handbook of Synchrotron Radiation*, by E.E. Koch (ed.) (North Holland, Amsterdam, 1993)
42. J.W.M. DuMond, Phys. Rev. **52**, 872 (1937)
43. Yu. Shvyd'ko, in *X-Ray Optics, High-Energy-Resolution Applications*, Springer Series in Optical Sciences vol. 98 (Springer, Berlin Heidelberg New York, 2004)
44. R. Follath, AIP Conf. Proc. 879-I, 513 (2007)